ACS OMEGA

Article

Cite This: ACS Omega 2018, 3, 11655−11662

http://pubs.acs.org/journal/acsodf

# Band-Like Charge Transport in $Cs_2AgBiBr_6$ and Mixed Antimony−Bismuth $Cs_2AgBi_{1-x}Sb_xBr_6$ Halide Double Perovskites

Eline M. Hutter,*[,†,‡] María C. Gélvez-Rueda,[‡] Davide Bartesaghi,[‡] Ferdinand C. Grozema,[‡] and Tom J. Savenije*[,‡]

[†]Department of Chemistry, Stanford University, Stanford, California 94305, United States

[‡]Department of Chemical Engineering, Delft University of Technology, Van der Maasweg 9, 2629 HZ Delft, The Netherlands

Supporting Information

**ABSTRACT:** Recently, halide double perovskites (HDPs), such as $Cs_2AgBiBr_6$, have been reported as promising nontoxic alternatives to lead halide perovskites. However, it remains unclear whether the charge-transport properties of these materials are as favorable as for lead-based perovskites. In this work, we study the mobilities of charges in $Cs_2AgBiBr_6$ and in mixed antimony−bismuth $Cs_2AgBi_{1-x}Sb_xBr_6$, in which the band gap is tunable from 2.0 to 1.6 eV. Using temperature-dependent time-resolved microwave conductivity techniques, we find that the mobility is proportional to $T^{-p}$ (with $p \approx 1.5$). Importantly, this indicates that phonon scattering is the dominant scattering mechanism determining the charge carrier mobility in these HDPs similar to the state-of-the-art lead-based perovskites. Finally, we show that wet chemical processing of $Cs_2AgBi_{1-x}Sb_xBr_6$ powders is a successful route to prepare thin films of these materials, which paves the way toward photovoltaic devices based on nontoxic HDPs with tunable band gaps.

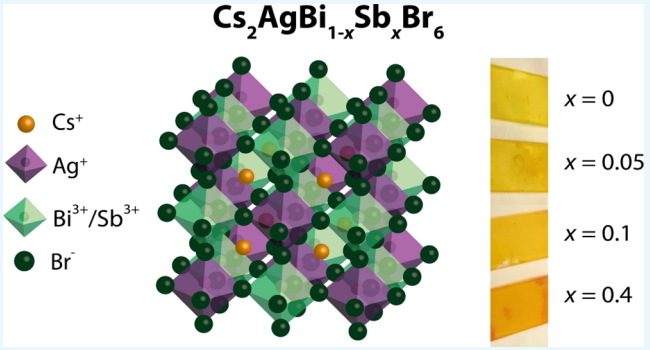


## 1. INTRODUCTION

Halide double perovskites (HDPs) such as $Cs_2AgBiBr_6$ have recently emerged as a nontoxic alternative to lead-based perovskites[1−5] and were successfully applied as radiation absorbers both in sensitive X-ray detectors and in photovoltaic devices.[6−8] Still, the power conversion efficiencies of $Cs_2AgBiBr_6$-based solar cells are relatively low,[7,8] which can be partially understood from its poor visible light absorption because of its indirect band gap of 2.19 eV.[2] It was recently shown that alloying $Tl^{3+}$ or $Sb^{3+}$, both thought to substitute for $Bi^{3+}$, can be used as a strategy to decrease the band gap of $Cs_2AgBiBr_6$ toward values more relevant for single-junction solar cells.[9,10] However, to date, there have been no reports presenting synthesis routes to prepare thin films of alloyed HDPs, which is a crucial step toward devices of these materials. Furthermore, although HDPs of various compositions have been designed,[9−13] it remains unclear whether the transport properties of these HDPs are as favorable as for their lead-based analogues.

In this work, we study the optoelectronic properties of $Cs_2AgBiBr_6$ and mixed antimony−bismuth HDPs with the general formula $Cs_2AgBi_{1-x}Sb_xBr_6$, which show an absorption red shift with increasing $x$, reaching ∼1.6 eV upon replacing 40% of the $Bi^{3+}$ with $Sb^{3+}$ (i.e. $x$ = 0.4).[10] We use pulse-radiolysis time-resolved microwave conductivity (PR-TRMC) measurements to gain insight in the mobility of free charges as a function of $x$ and temperature.[14−16] Interestingly, we find that the charge carrier mobility decreases only marginally on increasing $x$. Furthermore, we observe that, independent of the antimony content, the mobility decreases with increasing temperature in between 140 and 420 K. Importantly, the dependence of the mobility on temperature ($T^{-p}$, with $p \approx 1.5$) indicates band-like transport of charges in both $Cs_2AgBiBr_6$ and mixed antimony−bismuth analogues, in which the mobility is limited by phonon scattering. The observation that the charge-transport mechanism in these HDPs is very similar to lead-based perovskites,[17−19] highlights their potential as nontoxic alternatives. Finally, we find that dissolving the mixed antimony−bismuth HDP powders, synthesized using solid-state reactions, is a successful route to spin-coat thin $Cs_2AgBi_{1-x}Sb_xBr_6$ films. The preparation of thin HDP films with mixed trivalent metals paves the way toward photovoltaic devices based on HDPs with tunable band gaps.

## 2. RESULTS AND DISCUSSION

**2.1. Powders of $Cs_2AgBi_{1-x}Sb_xBr_6$.** Powders of $Cs_2AgBi_{1-x}Sb_xBr_6$, with $x$ values ranging from 0 to 0.4, were prepared from stoichiometric mixtures of the precursors CsBr, AgBr, $BiBr_3$, and $SbBr_3$, following previously reported solid-

Received: July 19, 2018
Accepted: September 10, 2018
Published: September 24, 2018




DOI: 10.1021/acsomega.8b01705
ACS Omega 2018, 3, 11655−11662

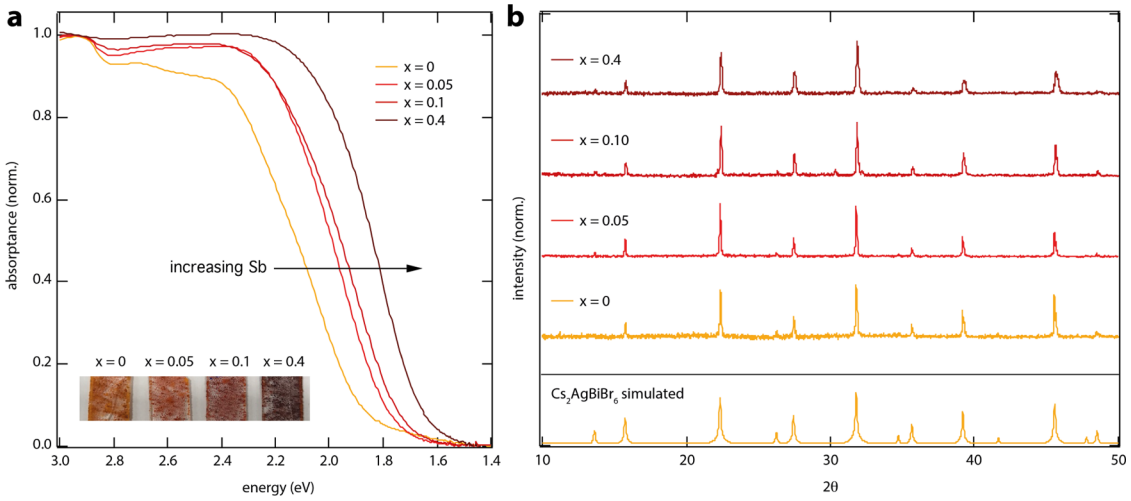


**Figure 1.** (a) Absorptance spectra normalized to unity to account for different surface coverages and (b) powder X-ray diffraction (XRD) patterns (Cu K$\alpha$ radiation, $\lambda$ = 1.54 Å) of mixed antimony−bismuth HDP powders with the general formula $Cs_2AgBi_{1-x}Sb_xBr_6$. Inset shows images of the powders with different Sb content.

state reaction procedures.[10] Here, $x$ represents the amount of $SbBr_3$ added to the reaction mixture, and the formulas are written assuming full substitution at the Bi site. The content of Sb in each sample was estimated using X-ray photoelectron spectroscopy (XPS). Although some variation across the sample is observed, we find that the Sb-to-Bi ratio increases monotonically with increasing Sb content in the precursors (see Supporting Information Table S1). Figure 1a shows the absorption spectra, measured using an integrating sphere, of $Cs_2AgBi_{1-x}Sb_xBr_6$ powders with $x$ = 0, 0.05, 0.1, and 0.4, attached to quartz substrates using optically clear adhesive. Consistent with the previous reports,[10,11] these spectra show that increasing the Sb content gradually reduces the band gap, resulting in absorption onset values close to 1.6 eV for $x$ = 0.4. Furthermore, all of the samples show X-ray reflections characteristic of the double perovskite structure, see Figure 1b, which monotonically shifts to larger angles on increasing $x$ (see also Supporting Information Figure S1), supporting the replacement of $Bi^{3+}$ with the smaller $Sb^{3+}$.

To investigate the suitability of $Cs_2AgBiBr_6$ and mixed antimony−bismuth HDPs for photovoltaic applications, we studied the transport of free charges in powders of these materials using the PR-TRMC technique.[14,15] With the PR-TRMC technique, free charges are homogeneously generated throughout the sample by irradiation with a high-energy electron pulse. These primary electrons are not injected but lose a part of their energy by ionizing the sample, resulting in a uniform distribution of electrons and holes. The density of charges initially generated by each high-energy electron from the pulse can be calculated using previously reported procedures (see Experimental Methods). The total density of free charges $n_0$ created by the electron pulse can be varied by changing its duration. A microwave probe is then used to measure the change in conductivity on the generation of free charges, which scales with the number and mobility ($\mu$) of charge carriers.[14,16] Importantly, because the initial density of free charges can be tuned independently of the exciton binding energy, the PR-TRMC technique is very suitable to determine the temperature-dependent mobility. Similar to the more widely used laser-induced TRMC,[20,21] the end-of-pulse charge density $n$ can however still be affected by fast trapping or recombination of mobile charges within the instrumental response time of 1 ns. Therefore, we choose a pulse length at which losses are minimized so that $n/n_0$ is closest to unity. Figure 2a shows the sum of electron and hole mobility $\sum\mu$ for $Cs_2AgBi_{1-x}Sb_xBr_6$ with $x$ = 0, 0.05, 0.1, and 0.4 at temperatures ranging from 140 to 420 K. From here, we find that at room temperature, $\sum\mu$ is at least 0.3 $cm^2/(V\,s)$ for $Cs_2AgBiBr_6$ ($x$ = 0) powders, which is only about four times lower than the mobility observed in $CsPbBr_3$ crystals using the same technique.[15,20]

The lower mobilities observed in $Cs_2AgBiBr_6$ are consistent with the effective masses of electrons and holes being somewhat larger than those for its lead-based analogue (i.e., $CsPbBr_3$).[4,22] In addition, the scattering times may be shorter because of enhanced scattering with phonons or defects. On partially replacing the $Bi^{3+}$ with $Sb^{3+}$, slightly reduced mobilities are observed, although at each temperature, the absolute values stay within the same order of magnitude. Furthermore, independent of $x$, the mobility decreases with rising temperatures in between 140 and 420 K. On further analysis of the data, we find that $\sum\mu$ scales with $T^{-1.15}$ for $x$ = 0, $T^{-1.62}$ ($x$ = 0.05), $T^{-1.19}$ ($x$ = 0.1), and $T^{-1.34}$ ($x$ = 0.4). Importantly, these negative powers indicate that phonon scattering (i.e., $\mu \propto T^{-1.5}$) is the dominant scattering mechanism determining the charge carrier mobility in these HDPs. These powers are within the same range as the state-of-the-art lead-based perovskites, for which values in between −1.2 and −1.6 have been reported.[17,19,23,24] Additionally, the observation that these negative powers are very similar for different $x$ values suggests that the charge-transport mechanism is not substantially disturbed on mixing bismuth with antimony. This means that independent of the $Sb^{3+}$ content in the $Cs_2AgBiBr_6$ lattice, there is band-like transport of charges with no indication of substantial defect scattering.

As mentioned above, charge carrier losses within the instrumental response time lead to a reduction of $n/n_0$. Therefore, to get insight into sub-nanosecond recombination processes, we can plot $(n/n_0)\sum\mu$ as a function of $n_0$ ($cm^{-3}$). This is shown in Figure 2b for $Cs_2AgBiBr_6$ (upper panel) and $Cs_2AgBi_{0.9}Sb_{0.1}Br_6$ (lower panel) for temperatures ranging from 140 to 420 K. At each temperature, $(n/n_0)\sum\mu$ initially



DOI: 10.1021/acsomega.8b01705
ACS Omega 2018, 3, 11655−11662

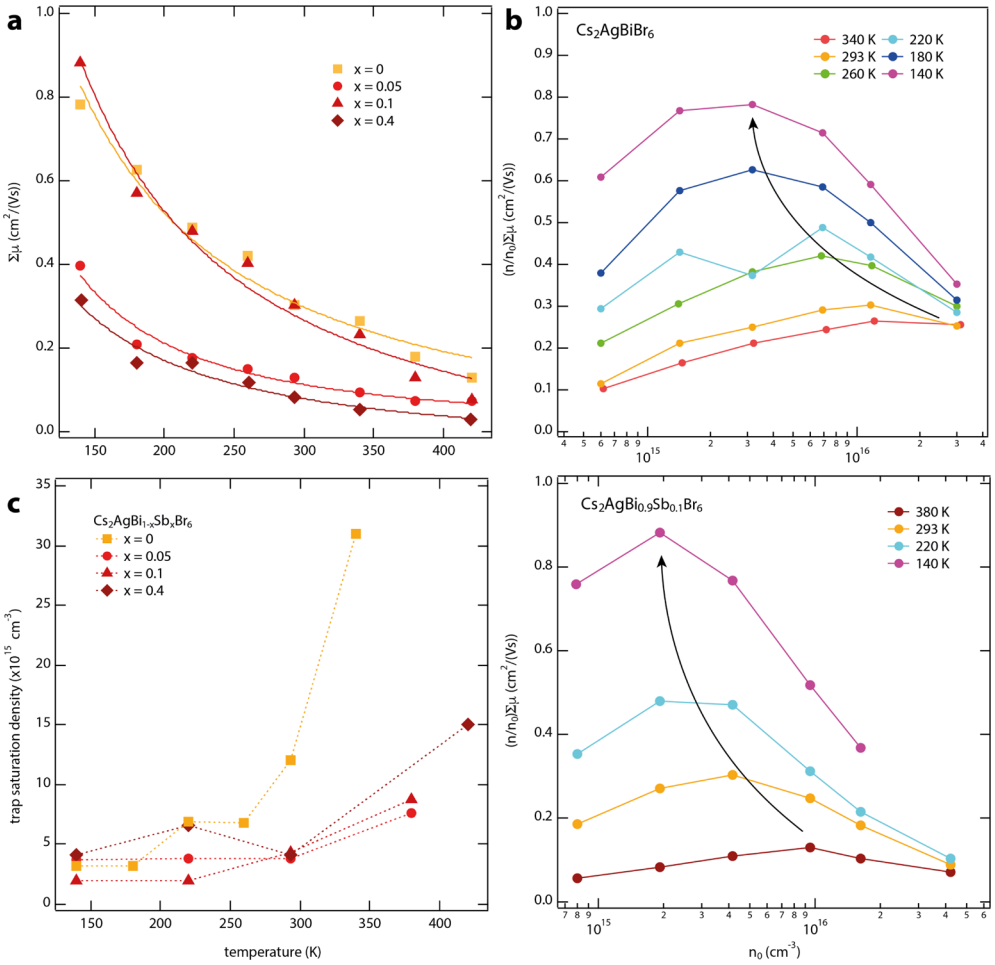


**Figure 2.** (a) Dots: mobility $\sum\mu$ as function of temperature for $x = 0$ (squares), $x = 0.05$ (spheres), $x = 0.1$ (triangles), and $x = 0.4$ (diamonds), determined using the PR-TRMC technique. On fitting these mobilities to $\mu(T) \propto T^{-p}$, added as solid lines, we obtained $p$-values of 1.15 ($x = 0$), 1.62 ($x = 0.05$), 1.19 ($x = 0.1$), and 1.34 ($x = 0.4$). (b) $(n/n_0)\sum\mu$ as function of $n_0$ and temperature for $x = 0$ (top) and $x = 0.1$ (bottom). (c) Trap saturation density as a function of temperature for $x = 0$ (squares), $x = 0.05$ (spheres), $x = 0.1$ (triangles), and $x = 0.4$ (diamonds), obtained from the maximum $n/n_0$.

rises on increasing the charge carrier densities. We attribute this to sub-nanosecond charge carrier trapping, leading to low yields if the trap density is higher than the charge carrier density.[25,26] Gradual saturation of these traps then results in increased $n$ values for higher $n_0$, and thus an enhancement of $n/n_0$. On further increasing $n_0$, $n/n_0$ decreases again, which is typically observed if higher order recombination starts to dominate.[27,28] Therefore, the charge carrier concentration at which $(n/n_0)\sum\mu$ reaches maximum values represents the regime in which band-to-band recombination is in competition with trap-assisted recombination and can thus be used as an indication of the trap saturation density ($cm^{-3}$).

Figure 2c displays the densities at which the traps are saturated as a function of temperature for the sample with ($x > 0$) and without ($x = 0$) antimony. For $Cs_2AgBiBr_6$, this shows a clear increase from $3 \times 10^{15}$ $cm^{-3}$ at 140 K to more than $3 \times 10^{16}$ $cm^{-3}$ for $T > 340$ K. The room-temperature value of $1.2 \times 10^{16}$ $cm^{-3}$ is close to the previously suggested upper limit of $10^{16}$ $cm^{-3}$ for a $Cs_2AgBiBr_6$ single crystal.[29] Interestingly, the temperature dependence of $(n/n_0)_{max}$ suggests that the trap density is enhanced with increasing temperatures, which could be because the origin of the traps is related to vacancies or interstitials, resulting from thermal displacement of ions. Alternatively, it might be that trap states originate from thermal ionization of defects, which also results in an increased number of available traps at higher temperatures. For the Sb-containing HDPs, the trap saturation densities at 140 K are $2-4 \times 10^{15}$ $cm^{-3}$ and thus close to the antimony-free $Cs_2AgBiBr_6$. Also here, an enhancement is observed as the temperature rises, with $(n/n_0)$ reaching a maximum just below $10^{16}$ $cm^{-3}$ at 380 K for $Cs_2AgBi_{0.9}Sb_{0.1}Br_6$ (see bottom panel in Figure 2b) and the other mixed antimony–bismuth HDP powders (see also Supporting Information Figure S2). Most importantly, at and above room temperature, the trap-saturation densities for $x > 0$ are about a factor three lower than that for $x = 0$, see Figure 2c. If indeed the trap states in $Cs_2AgBiBr_6$ are related to thermal ionic motion or defect ionization, these results suggest that this can be partially suppressed by $Sb^{3+}$ substitution.

**2.2. Thin Films of $Cs_2AgBi_{1-x}Sb_xBr_6$.** The preparation of thin films of alloyed HDPs is a crucial step toward devices employing HDPs with tunable band gaps and also important to further investigate their optoelectronic properties using spectroscopic techniques.[30] Although it was recently shown that $Cs_2AgBiBr_6$ films can be spin-coated from a solution of its precursors in dimethyl sulfoxide (DMSO),[7] there have been no reports on mixed trivalent metal HDP films. Here, we used the products of the solid-state synthesis to prepare thin films of $Cs_2AgBi_{1-x}Sb_xBr_6$, see also Experimental Methods. These



DOI: 10.1021/acsomega.8b01705
ACS Omega 2018, 3, 11655−11662

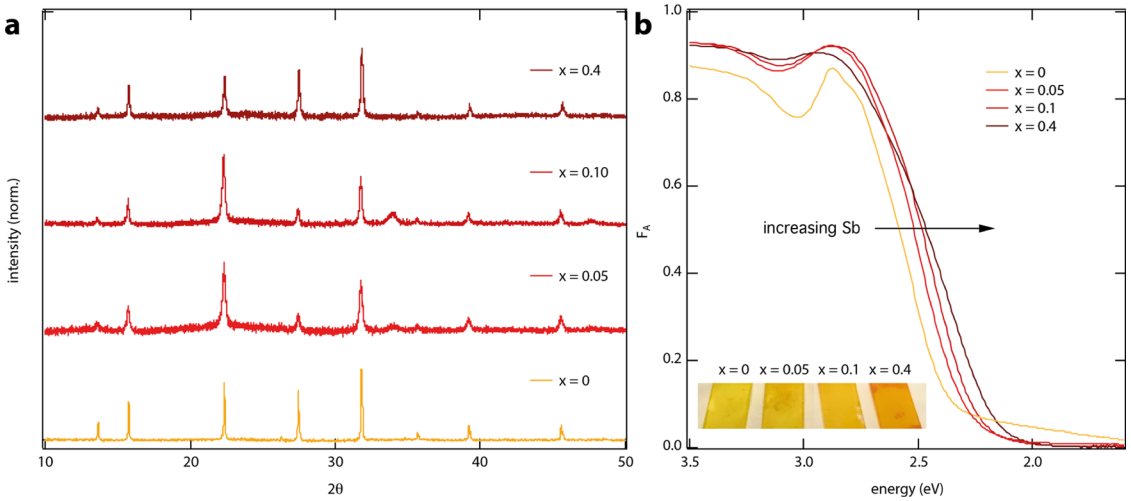


**Figure 3.** (a) XRD patterns and (b) absorptance spectra of thin $Cs_2AgBi_{1-x}Sb_xBr_6$ films, spin-coated from solutions of the powders (0.5 M) in DMSO.

powders were dissolved in DMSO at 0.5 M, yielding clear solutions with yellow to orange color (depending on $x$). The solutions, preheated to 75 °C, were then spin-coated on quartz substrates, followed by annealing at 200 °C ($x$ = 0)[7] or 90 °C (for $x$ > 0). Note that we used lower annealing temperatures for the Sb-containing films, as we noticed the formation of undesired side phases (such as $Cs_3Sb_2Br_9$) on using high annealing temperatures (see Supporting Information Figure S4).

Figure 3a shows the XRD patterns of the resulting films with $x$ = 0, 0.05, 0.1, and 0.4, showing all of the reflections characteristic of the HDP crystal structure. The shift to higher angles (see also Supporting Information Figure S5) shows that the lattice parameters are reduced on addition of Sb, consistent with $Sb^{3+}$ replacing the larger $Bi^{3+}$ in these HDP thin films. In addition, we observe that the reflections are broader for $x$ > 0 than that for $x$ = 0, suggesting that the crystalline domains are larger for the latter. Note that the different relative intensities of the reflections compared to the corresponding powders (Figure 2c) most likely result from preferential orientations of the crystalline domains with respect to the substrate. XPS analysis (Supporting Information Figure S6 and Table S2) of the thin films indicates higher Sb fractions for increasing $x$, which we find to be homogeneously distributed according to the scanning electron microscopy−energy dispersive X-ray spectroscopy analysis (Supporting Information Figure S7).

Figure 3b shows the absorptance (i.e., attenuation) spectra of the thin films. Although we expect the absorption coefficients to be identical, the absorption onsets for the submicron thick films and for the corresponding millimeter-sized powders are very different. This can be attributed to the low absorption coefficients close to the (indirect) band gap of these materials, which makes the onset of the absorptance very sensitive for the sample thickness (see Supporting Information Figure S8 for the absorption coefficients of $Cs_2AgBi_{1-x}Sb_xBr_6$ for $x$ = 0 and $x$ = 0.4).[1,10] However, consistent with the $Cs_2AgBi_{1-x}Sb_xBr_6$ powders, the absorption onset of the films is red-shifted on increasing $x$, indicating that alloying $Bi^{3+}$ and $Sb^{3+}$ is an effective strategy to manipulate the band gap in thin HDP films. Altogether, the above results indicate that the Sb substitution in antimony−bismuth alloyed thin films increases when using higher values of $x$, although we note that the absolute stoichiometry in the films might deviate from the powders, as indicated by nonmonotonic shifts in the XRD patterns (see Supporting Information Figure S5).

To investigate to what extent the PR-TRMC results of the antimony−bismuth alloyed HDP powders (Figure 2) are representative for light-generated charges in the thin $Cs_2AgBi_{1-x}Sb_xBr_6$ films, we recorded the photoconductance using laser-induced TRMC measurements.[20,21] Figure 4 shows the photoconductance as a function of time for the $Cs_2AgBiBr_6$ (Figure 4a) and $Cs_2AgBi_{0.6}Sb_{0.4}Br_6$ (Figure 4b) films, using an excitation energy of 2.8 eV. Here, the maximum signal height represents the yield-mobility product $\varphi\sum\mu$, in which the yield $\varphi$ represents the ratio between free charges and absorbed photons.[21] For $Cs_2AgBiBr_6$ (Figure 4a), consistent with the PR-TRMC measurements, we initially observe an enhancement of the maximum signal height (i.e., $\varphi\sum\mu$), followed by a decrease on further increasing the excitation density in $Cs_2AgBiBr_6$ (Figure 4a). Interestingly, the maximum $\varphi\sum\mu$ is found at a charge density $1 \times 10^{16}$ $cm^{-3}$, meaning that the density at which the traps are saturated in these thin films is nearly identical to that of the corresponding powders (i.e., $1.2 \times 10^{16}$ $cm^{-3}$ at room temperature, recall Figure 2c).

We can further conclude from the maximum $\varphi\sum\mu$ that the sum of the electron and hole mobilities amounts to at least 0.8 $cm^2/(V\ s)$ for the nonalloyed HDP (Figure 4a, $x$ = 0), similar to previously reported values for a $Cs_2AgBiBr_6$ thin film.[29] This relatively low mobility value compared to lead-based perovskites is in agreement with the larger effective masses of both electrons and holes.[4] The photoconductance signals decay at time scales on the order of a microsecond, which suggests that the microsecond lifetime recently observed using transient absorption spectroscopy on similar samples originates at least partially from mobile charges.[30] We note that this observation is in contrast with our previous TRMC results, which showed that all mobile charges recombined within several nanoseconds after exciting a $Cs_2AgBiBr_6$ film synthesized under ambient conditions.[29] We suspect that the longer recombination lifetimes in the films of the current work are due to the fact that all of these samples were synthesized under inert conditions and not exposed to air at any time before or during the measurements. The microsecond lifetimes in $Cs_2AgBiBr_6$ films synthesized under inert conditions (Figure



DOI: 10.1021/acsomega.8b01705
ACS Omega 2018, 3, 11655−11662

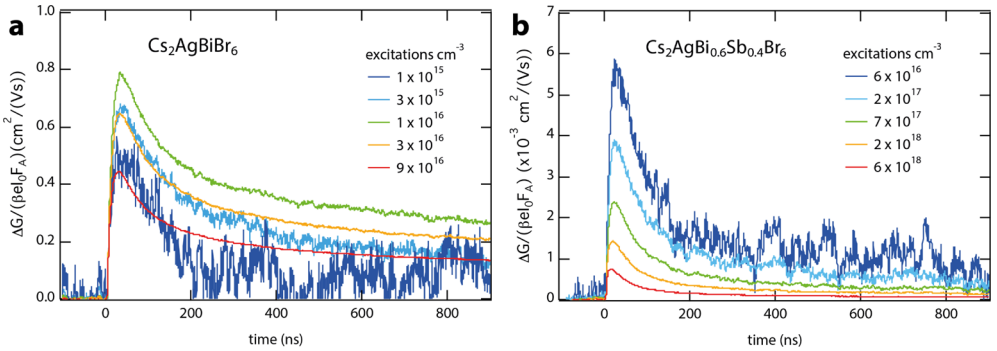


**Figure 4.** Photoconductance as a function of time after excitation at 2.8 eV for $Cs_2AgBiBr_6$ (a) and $Cs_2AgBi_{0.6}Sb_{0.4}Br_6$ (b).

4a) suggest that at least one of the charges remains free, and that the decay represents the recombination between a free charge and its trapped counter-charge. On the basis of the mobility and half lifetime, we estimate that the diffusion length of the free charge carrier in $Cs_2AgBiBr_6$ thin film amounts to 0.6 $\mu$m (see Supporting Information Table S3). Although this is relatively short compared to fully optimized state-of-the-art lead-based perovskites,[15,27] this value suggests that $Cs_2AgBiBr_6$ is a potential nontoxic alternatives to lead-based perovskites.

For the $Cs_2AgBi_{0.6}Sb_{0.4}Br_6$ (Figure 4b) thin film, the $\varphi\sum\mu$ decreases on increasing the charge density from $6 \times 10^{16}$ to $6 \times 10^{18}$ $cm^{-3}$, indicating that higher order recombination processes dominate in this regime.[28] Additionally, the maximum $\varphi\sum\mu$ is 2 orders of magnitude smaller than for the antimony-free HDP film (Figure 4a). On measuring the corresponding powders with laser-induced TRMC, we also obtained lower photoconductance signals for the Sb-containing HDPs (Supporting Information Figure S9), although here the difference in $\varphi\sum\mu$ is 1 order of magnitude. This can at least partially be explained considering that the charge carrier lifetimes for $Cs_2AgBi_{1-x}Sb_xBr_6$ with $x = 0.4$ as observed by PR-TRMC traces, shown in Figure S3, are very short: less than 10 ns. Because the light-induced TRMC measurements make use of a cavity with a response time close to 18 ns, we can thus expect a severe reduction in $\varphi\sum\mu$. For thin films, however, the lower $\varphi\sum\mu$ on Sb substitution (Figure 4b) might also be because of a decreased $\sum\mu$ resulting from its smaller crystalline domain sizes.[31] In addition, the trap density might be higher in thin films, for instance, because of oxidation of a small fraction of $Sb^{3+}$, which we are currently investigating. However, in view of the well-preserved charge-transport properties for the Sb-substituted $Cs_2AgBiBr_6$ powders (Figure 2), it seems likely that further optimizing the synthesis procedure and annealing conditions will improve the sample quality and hence increase both mobilities and lifetimes in thin films of Sb-containing HDPs. Finally, we want to highlight that the introduction of Sb results in a band gap narrowing instead of the formation of intra band gap defect states. On excitation of $Cs_2AgBi_{1-x}Sb_xBr_6$ ($x = 0.4$) powder at 1.7 eV, which is below the onset of $Cs_2AgBiBr_6$, the maximum TRMC signal heights and thus $\varphi\sum\mu$ are similar to those obtained at 2.8 eV, as shown in Figure S9. Similar results are obtained for the films.

## 3. CONCLUSIONS

To summarize, we have investigated the optoelectronic properties of the double-perovskite $Cs_2AgBiBr_6$ and mixed antimony-bismuth HDPs with the general formula $Cs_2AgBi_{1-x}Sb_xBr_6$, in which the band gap can be tuned from 2.0 to 1.6 eV by increasing the antimony content. With PR-TRMC measurements on $Cs_2AgBi_{1-x}Sb_xBr_6$ powders, we observe that for all $x$ values, the charge carrier mobility increases on decreasing the temperature. The power law dependence of the mobilities on temperature show that phonon scattering (i.e., $\mu \propto T^{-1.5}$) is the dominant scattering mechanism determining the charge-carrier mobility in these HDPs. Importantly, these results show that for both $Cs_2AgBiBr_6$ and mixed trivalent metal $Cs_2AgBi_{1-x}Sb_xBr_6$, the charge-transport mechanism is similar to the state-of-the-art lead-based perovskites. The combination of band-like transport and band gap tunability in $Cs_2AgBi_{1-x}Sb_xBr_6$ highlights the potential of these materials as nontoxic alternatives to lead-based perovskites. Finally, we demonstrate the preparation of thin films of $Cs_2AgBi_{1-x}Sb_xBr_6$, showing that the incorporation of Sb can red shift the absorption onset up to a few 100 meV in thin $Cs_2AgBiBr_6$ films. Altogether, these results represent a crucial step toward lead-free perovskite devices implementing antimony−bismuth-alloyed HDPs.

## 4. EXPERIMENTAL METHODS

**4.1. $Cs_2AgBi_{1-x}Sb_xBr_6$ Powders.** CsBr (1 mmol), 0.5 mmol AgBr, $(1 - x)0.5$ mmol $BiBr_3$, and $0.5x$ mmol $SbBr_3$ were ground until fine powders were obtained. The mixtures were sealed in glass tubes under vacuum and heated in a box furnace to 320 °C (heating rate of 3 °C/min) and kept at this temperature for 3 h.[10] After cooling down to room temperature (cooling rate of 3 °C/min), the closed tubes containing the products were transferred to a nitrogen-filled glovebox. For this work, $x$ was varied between 0 and 0.4; attempts to prepare higher concentrations of $x$ failed.

**4.2. $Cs_2AgBi_{1-x}Sb_xBr_6$ Thin Films.** $Cs_2AgBi_{1-x}Sb_xBr_6$ (0.5 mmol) was dissolved in 1 mL of DMSO at 75 °C under magnetic stirring in a nitrogen-filled glovebox.[7] Quartz substrates were cleaned with isopropanol and treated with an ozone plasma for 30 min. The $Cs_2AgBi_{1-x}Sb_xBr_6$/DMSO solutions were filtered and kept at 75 °C. Then, 100 $\mu$L of the filtered solution was spin-coated on a quartz substrate using a two-step procedure starting at 500 rpm for 30 s (ramping speed of 100 rpm/s), followed by 60 s at 5000 rpm (ramping speed of 5000 rpm/s). The $Cs_2AgBiBr_6$ ($x = 0$) films were annealed at 200 °C for 3 min, and the Sb-containing films were annealed at 90 °C for 3 min.

**4.3. X-ray Diffraction.** XRD patterns were obtained with a Bruker D8 diffractometer in a Bragg−Brentano configuration, using Cu K$\alpha$ ($\lambda$ = 1.54 Å) radiation.

**4.4. X-ray Photoelectron Spectroscopy.** XPS measurements were performed with a Thermo Scientific K-alpha



DOI: 10.1021/acsomega.8b01705
ACS Omega 2018, 3, 11655−11662

instrument, equipped with an Al K$\alpha$ X-ray source and a flood gun to avoid charging of the sample. For the high-resolution scans of C 1s, O 1s, Ag 3d, Bi 4f, Br 3d, Sb 3d, and Cs 3d signals, the following parameters were used: spot size of 400 $\mu$m, pass energy of 50 eV, energy step size of 0.1 eV, dwell time of 50 ms, and 10 scans. XPS spectra were corrected using the atmospheric carbon C peak position (284.8 eV). Elemental quantification was performed using the Avantage software. High-resolution scans of each element were fit with a mixture of Gaussian and Lorentzian functions; the area under each peak was used to determine the concentration of each element.

**4.5. Optical Characterization.** Absorption and transmission spectra were recorded with a PerkinElmer Lambda 1050 spectrophotometer equipped with an integrated sphere. The thin $Cs_2AgBi_{1-x}Sb_xBr_6$ films were placed in front of the sphere to measure the fraction of the transmitted light ($F_T$) and under an angle of 10° inside the sphere to detect the total fraction of reflected and transmitted photons ($F_{R+T}$). From here, we calculated the fraction of absorbed light (absorptance; $F_A$)

$$F_A = 1 - F_{T+R}$$

The fraction of reflected light ($F_R$) was determined from

$$F_R = 1 - F_A - F_T$$

The absorption coefficient $\alpha$ is often calculated from the transmission spectrum using

$$\frac{I_L}{I_0} = e^{-\alpha L}$$

where $I_L/I_0$ equals $F_T$ for a sample of thickness $L$ with a negligible reflection. However, since thin perovskite films are highly reflective, $\alpha$ was obtained from

$$\frac{F_T}{1 - F_R} = e^{-\alpha L}$$

The $Cs_2AgBi_{1-x}Sb_xBr_6$ powders were attached to quartz substrates using optically clear adhesive tape (Thorlabs), and the fraction of absorbed light was determined from the experimental $F_{R+T}$, as described above.

**4.6. PR-TRMC Measurements.** About 30 mg of each $Cs_2AgBi_{1-x}Sb_xBr_6$ powder was put in a sample holder and covered with polymethyl methacrylate (PMMA), drop-casted from a 10 mg/mL PMMA/chlorobenzene solution, to protect from moisture and air. PR-TRMC measurements involve the generation of charge carriers through irradiation by a short pulse of high-energy electrons (3 MeV) and the monitoring of the changes in conductivity because of mobile charge carriers using high-frequency microwaves (28−38 GHz).[14,16] The change in conductivity is proportional to the absorbed microwave power via a sensitivity factor $A$

$$\frac{\Delta P}{P} = A\Delta\sigma$$

The experimental frequency dependence of $\Delta P/P$ can be fitted with an analytical expression to determine the dielectric constant, $\varepsilon$, and change in conductivity, $\Delta\sigma$.[14]

The mobility is then calculated by

$$\Delta\sigma = e\sum n_0\mu$$

where $n_0$ is the initial concentration of charge carriers at the end of the pulse and $\mu$ is the sum of the mobilities for electrons and holes. $n_0$ is a function of the mass of material ($m$), volume of the sample holder ($V_{sh}$), irradiation energy deposited in the sample ($D$), and the radiation-ionization energy required for the generation of an electron−hole pair ($E_p$)

$$n_0 = \frac{D}{E_p \times 1.6 \times 10^{-19}\ \text{J/eV}}\frac{m}{V_{sh}}$$

$D$ is proportional to the electron density of the material, and perovskites has been determined to be ∼1 J/kg/nC.[15] The latter is derived from previous radiation dosimetry experiments. $E_p$ has been determined according to Klein's theoretical model[32] and Alig's equation[33] for semiconductor materials, which relates it to the band gap of the material, phonon losses, and the residual kinetic energy

$$E_p = 2.73E_g + 0.55\ \text{(eV)}$$

In the PR-TRMC setup, the cell is contained in a cryostat in which the temperature can be varied between 123 and 473 K. The temperature was maintained for ∼15 min before doing the actual measurement to assure the equilibrium of the system. The overall time response of the setup is limited by the rise time of the detector diode and the length of the excitation pulse (∼1 ns).

**4.7. Laser-Induced TRMC Measurements.** The thin films on quartz substrates were placed in an airtight microwave cell inside a $N_2$-filled glovebox. The TRMC technique was used to measure the change in microwave (8.5 GHz) power after pulsed excitation (repetition rate 10 Hz) of the samples at various excitation wavelengths. Neutral density filters were used to vary the intensity of the incident light. The illuminated sample area is ∼2.5 cm$^2$. The time-resolved change in conductance $\Delta G(t)$ was obtained from the photoexcitation-induced change in microwave power $\Delta P(t)$, which are related by a sensitivity factor $K$[21]

$$\frac{\Delta P(t)}{P} = -K\Delta G(t)$$

The rise of $\Delta G$ is limited by the width of the laser pulse (3.5 ns full width at half maximum) and the response time of our microwave system (18 ns). The slow repetition rate of the laser of 10 Hz ensures full relaxation of all photoinduced charges to the ground state before the next laser pulse hits the sample. Before and during the photoconductance measurements, the samples were not exposed to moisture and air to prevent degradation.

## ■ ASSOCIATED CONTENT

### Supporting Information

The Supporting Information is available free of charge on the ACS Publications website at DOI: 10.1021/acsomega.8b01705.

Elemental analysis, XRD, and additional TRMC data (PDF)

## ■ AUTHOR INFORMATION


### Corresponding Authors

*E-mail: E.M.Hutter@tudelft.nl (E.M.H.).
*E-mail: T.J.Savenije@tudelft.nl (T.J.S.).

### ORCID

Eline M. Hutter: 0000-0002-5537-6545
Davide Bartesaghi: 0000-0002-7467-269X




DOI: 10.1021/acsomega.8b01705
ACS Omega 2018, 3, 11655−11662

Ferdinand C. Grozema: 0000-0002-4375-799X
Tom J. Savenije: 0000-0003-1435-9885

### Notes

The authors declare no competing financial interest.

## ■ ACKNOWLEDGMENTS

Hemamala Karunadasa is acknowledged for facilitating this project and for critical reading of this manuscript. The authors thank Adam Slavney for fruitful discussions. This work was supported by the Netherlands Organization for Scientific Research (NWO) under the Echo grant number: 712.014.007. E.M.H. received additional funding via a Fulbright Scholarship. Work by D.B. was funded by the Partnership Program of the Materials Innovation Institute M2i and the Foundation of Fundamental Research on Matter, Netherlands Organization for Scientific Research (F71.4.15562a).

## ■ REFERENCES

(1) Slavney, A. H.; Hu, T.; Lindenberg, A. M.; Karunadasa, H. I. A Bismuth-Halide Double Perovskite with Long Carrier Recombination Lifetime for Photovoltaic Applications. *J. Am. Chem. Soc.* **2016**, *138*, 2138−2141.

(2) McClure, E. T.; Ball, M. R.; Windl, W.; Woodward, P. M. Cs2AgBiX6 (X = Br, Cl): New Visible Light Absorbing, Lead-Free Halide Perovskite Semiconductors. *Chem. Mater.* **2016**, *28*, 1348−1354.

(3) Han, K.; Yang, B.; Chen, J.; Yang, S.; Hong, F.; Sun, L.; Han, P.; Pullerits, T.; Deng, W. Lead-Free Silver-Bismuth Halide Double Perovskite Nanocrystals. *Angew. Chem., Int. Ed.* **2018**, *130*, 5457−5461.

(4) Volonakis, G.; Filip, M. R.; Haghighirad, A. A.; Sakai, N.; Wenger, B.; Snaith, H. J.; Giustino, F. Lead-Free Halide Double Perovskites via Heterovalent Substitution of Noble Metals. *J. Phys. Chem. Lett.* **2016**, *7*, 1254−1259.

(5) Filip, M. R.; Hillman, S.; Haghighirad, A. A.; Snaith, H. J.; Giustino, F. Band Gaps of the Lead-Free Halide Double Perovskites Cs2BiAgCl6 and Cs2BiAgBr6 from Theory and Experiment. *J. Phys. Chem. Lett.* **2016**, *7*, 2579−2585.

(6) Pan, W.; Wu, H.; Luo, J.; Deng, Z.; Ge, C.; Chen, C.; Jiang, X.; Yin, W.-J.; Niu, G.; Zhu, L.; et al. Cs2AgBiBr6 Single-Crystal X-Ray Detectors with a Low Detection Limit. *Nat. Photonics* **2017**, *11*, 726−732.

(7) Greul, E.; Petrus, M. L.; Binek, A.; Docampo, P.; Bein, T. Highly Stable, Phase Pure Cs2AgBiBr6 Double Perovskite Thin Films for Optoelectronic Applications. *J. Mater. Chem. A* **2017**, *5*, 19972−19981.

(8) Pantaler, M.; Cho, K. T.; Queloz, V. I. E.; García Benito, I.; Fettkenhauer, C.; Anusca, I.; Nazeeruddin, M. K.; Lupascu, D. C.; Grancini, G. Hysteresis-Free Lead-Free Double-Perovskite Solar Cells by Interface Engineering. *ACS Energy Lett* **2018**, *3*, 1781−1786.

(9) Slavney, A. H.; Leppert, L.; Bartesaghi, D.; Gold-Parker, A.; Toney, M. F.; Savenije, T. J.; Neaton, J. B.; Karunadasa, H. I. Defect-Induced Band-Edge Reconstruction of a Bismuth-Halide Double Perovskite for Visible-Light Absorption. *J. Am. Chem. Soc.* **2017**, *139*, 5015−5018.

(10) Du, K.-z.; Meng, W.; Wang, X.; Yan, Y.; Mitzi, D. B. Bandgap Engineering of Lead-Free Double Perovskite Cs2 AgBiBr6 through Trivalent Metal Alloying. *Angew. Chem., Int. Ed.* **2017**, *56*, 8158−8162.

(11) Tran, T. T.; Panella, J. R.; Chamorro, J. R.; Morey, J. R.; McQueen, T. M. Designing Indirect-Direct Bandgap Transitions in Double Perovskites. *Mater. Horiz.* **2017**, *4*, 688−693.

(12) Du, K.-z.; Wang, X.; Han, Q.; Yan, Y.; Mitzi, D. B. Heterovalent B-Site Co-Alloying Approach for Halide Perovskite Bandgap Engineering. *ACS Energy Lett* **2017**, *2*, 2486−2490.

(13) Volonakis, G.; Haghighirad, A. A.; Milot, R. L.; Sio, W. H.; Filip, M. R.; Wenger, B.; Johnston, M. B.; Herz, L. M.; Snaith, H. J.; Giustino, F. Cs2InAgCl6: A New Lead-Free Halide Double Perovskite with Direct Band Gap. *J. Phys. Chem. Lett.* **2017**, *8*, 772−778.

(14) Warman, J. M.; de Haas, M. P.; Dicker, G.; Grozema, F. C.; Piris, J.; Debije, M. G. Charge Mobilities in Organic Semiconducting Materials Determined by Pulse-Radiolysis Time-Resolved Microwave Conductivity: π-Bond-Conjugated Polymers versus π−π-Stacked Discotics. *Chem. Mater.* **2004**, *16*, 4600−4609.

(15) Gélvez-Rueda, M. C.; Cao, D. H.; Patwardhan, S.; Renaud, N.; Stoumpos, C. C.; Schatz, G. C.; Hupp, J. T.; Farha, O. K.; Savenije, T. J.; Kanatzidis, M. G.; et al. Effect of Cation Rotation on Charge Dynamics in Hybrid Lead Halide Perovskites. *J. Phys. Chem. C* **2016**, *120*, 16577−16585.

(16) Grozema, F. C.; Siebbeles, L. D. A. Charge Mobilities in Conjugated Polymers Measured by Pulse Radiolysis Time-Resolved Microwave Conductivity: From Single Chains to Solids. *J. Phys. Chem. Lett.* **2011**, *2*, 2951−2958.

(17) Savenije, T. J.; Ponseca, C. S.; Kunneman, L.; Abdellah, M.; Zheng, K.; Tian, Y.; Zhu, Q.; Canton, S. E.; Scheblykin, I. G.; Pullerits, T.; et al. Thermally Activated Exciton Dissociation and Recombination Control the Carrier Dynamics in Organometal Halide Perovskite. *J. Phys. Chem. Lett.* **2014**, *5*, 2189−2194.

(18) Rehman, W.; Milot, R. L.; Eperon, G. E.; Wehrenfennig, C.; Boland, J. L.; Snaith, H. J.; Johnston, M. B.; Herz, L. M. Charge-Carrier Dynamics and Mobilities in Formamidinium Lead Mixed-Halide Perovskites. *Adv. Mater.* **2015**, *27*, 7938−7944.

(19) Karakus, M.; Jensen, S. A.; D'Angelo, F.; Turchinovich, D.; Bonn, M.; Cánovas, E. Phonon-Electron Scattering Limits Free Charge Mobility in Methylammonium Lead Iodide Perovskites. *J. Phys. Chem. Lett.* **2015**, *6*, 4991−4996.

(20) Hutter, E. M.; Gélvez-Rueda, M. C.; Osherov, A.; Bulović, V.; Grozema, F. C.; Stranks, S. D.; Savenije, T. J. Direct-Indirect Character of the Bandgap in Methylammonium Lead Iodide Perovskite. *Nat. Mater.* **2017**, *16*, 115−120.

(21) Savenije, T. J.; Ferguson, A. J.; Kopidakis, N.; Rumbles, G. Revealing the Dynamics of Charge Carriers in Polymer:Fullerene Blends Using Photoinduced Time-Resolved Microwave Conductivity. *J. Phys. Chem. C* **2013**, *117*, 24085−24103.

(22) Yin, J.; Maity, P.; De Bastiani, M.; Dursun, I.; Bakr, O. M.; Brédas, J.-L.; Mohammed, O. F. Molecular Behavior of Zero-Dimensional Perovskites. *Sci. Adv.* **2017**, *3*, e1701793.

(23) Milot, R. L.; Eperon, G. E.; Snaith, H. J.; Johnston, M. B.; Herz, L. M. Temperature-Dependent Charge-Carrier Dynamics in CH3NH3PbI3Perovskite Thin Films. *Adv. Funct. Mater.* **2015**, *25*, 6218−6227.

(24) Oga, H.; Saeki, A.; Ogomi, Y.; Hayase, S.; Seki, S. Improved Understanding of the Electronic and Energetic Landscapes of Perovskite Solar Cells: High Local Charge Carrier Mobility, Reduced Recombination, and Extremely Shallow Traps. *J. Am. Chem. Soc.* **2014**, *136*, 13818−13825.

(25) Hutter, E. M.; Sutton, R. J.; Chandrashekar, S.; Abdi-Jalebi, M.; Stranks, S. D.; Snaith, H. J.; Savenije, T. J. Vapour-Deposited Cesium Lead Iodide Perovskites: Microsecond Charge Carrier Lifetimes and Enhanced Photovoltaic Performance. *ACS Energy Lett.* **2017**, *2*, 1901−1908.

(26) Savenije, T. J.; Huijser, A.; Vermeulen, M. J. W.; Katoh, R. Charge Carrier Dynamics in TiO2 Nanoparticles at Various Temperatures. *Chem. Phys. Lett.* **2008**, *461*, 93−96.

(27) Hutter, E. M.; Eperon, G. E.; Stranks, S. D.; Savenije, T. J. Charge Carriers in Planar and Meso-Structured Organic-Inorganic Perovskites: Mobilities, Lifetimes, and Concentrations of Trap States. *J. Phys. Chem. Lett.* **2015**, *6*, 3082−3090.

(28) Labram, J. G.; Chabinyc, M. L. Recombination at High Carrier Density in Methylammonium Lead Iodide Studied Using Time-Resolved Microwave Conductivity. *J. Appl. Phys.* **2017**, *122*, 065501.

(29) Bartesaghi, D.; Slavney, A. H.; Gélvez-Rueda, M. C.; Connor, B. A.; Grozema, F. C.; Karunadasa, H. I.; Savenije, T. J. Charge Carrier Dynamics in Cs2AgBiBr6 Double Perovskite. *J. Phys. Chem. C* **2018**, *122*, 4809−4816.



DOI: 10.1021/acsomega.8b01705
*ACS Omega* 2018, 3, 11655−11662

(30) Hoye, R. L. Z.; Eyre, L.; Wei, F.; Brivio, F.; Sadhanala, A.; Sun, S.; Li, W.; Zhang, K. H. L.; MacManus-Driscoll, J. L.; Bristowe, P. D.; et al. Fundamental Carrier Lifetime Exceeding 1 $\mu$s in Cs2 AgBiBr6 Double Perovskite. *Adv. Mater. Interfaces* **2018**, *5*, 1800464.
(31) Reid, O. G.; Yang, M.; Kopidakis, N.; Zhu, K.; Rumbles, G. Grain-Size-Limited Mobility in Methylammonium Lead Iodide Perovskite Thin Films. *ACS Energy Lett* **2016**, *1*, 561−565.
(32) Klein, C. A. Bandgap Dependence and Related Features of Radiation Ionization Energies in Semiconductors. *J. Appl. Phys.* **1968**, *39*, 2029−2038.
(33) Alig, R. C.; Bloom, S. Electron-Hole-Pair Creation Energies in Semiconductors. *Phys. Rev. Lett.* **1975**, *35*, 1522−1525.



DOI: 10.1021/acsomega.8b01705
*ACS Omega* 2018, 3, 11655−11662